Contact Monitoring of Un-gelled Stainless-Steel ECG Electrodes

M. J. Burke, C. Molloy, and H. Fossan

***Abstract*—**A circuit is developed to measure the quality of contact of un-gelled stainless-steel ECG electrodes with the mother's skin in a heart rate monitor used during childbirth. The circuit measures the contact impedance continually and gives a visual indication of whether the impedance is above or below an acceptable threshold. The output signal interfaces with an ultrasonic heart rate transducer being used to measure the unborn infant's heart-rate. This allows the midwifery staff to ensure that the ultrasound monitor is actually measuring the infant's heart rate correctly and not that of the mother. The circuit developed measures the quality of contact of stainless-steel electrodes having contact impedance as high as 100kΩ using an injected signal at a frequency of 5 kHz. It assesses the contact of individual left and right electrodes independently.

***Keywords*—**Electrode impedance, un-gelled electrodes, heart rate monitoring, ECG amplifier.

I. Introduction

THE Safer Births Program [1], sponsored by the Norwegian Research Council as part of a larger World Health Organization initiative [2], is an action plan aimed at eliminating preventable deaths of infants at birth, with particular focus on developing countries. Many maternity units in these locations are understaffed and in some cases rely on midwives and nurses alone to contend with the complications that arise around birth, without proper access to the advanced medical assistance or equipment needed to deal with them. Few places have sufficient equipment for fetal monitoring such that fetuses in distress are left unattended, adding to the burden of birth asphyxia and stillbirth. Many of the infants born may not be breathing correctly, or at all, and have pulses which are difficult, and sometimes impossible, to detect manually. On occasions these infants can be misclassified as stillborn when, in fact, their hearts have not stopped functioning and they could be resuscitated with the help of suitable equipment. Laerdal Medical AS, a Norwegian company that manufactures medical training equipment, is currently extending its range of products to include resuscitation equipment for the scenarios described above. One such product is the Moyo unit shown in Fig 1. This unit is a fetal heart rate monitor which uses an ultrasonic transducer placed on the mother's abdomen to detect the infant's heart beat and indicates the fetal heart rate on a LCD display. One common problem with ultrasonic heart rate monitors is that when the infant's heart beat is difficult to detect the transducer often picks up the mother's heart rate in error [3]. In order to overcome this problem the Moyo unit incorporates an ECG amplifier and circuitry which can be used to measure the mother's heart rate by way of her ECG and to indicate this on a separate LCD display. The Moyo unit is held by the mother giving birth and, when requested to do so, she presses her fingers onto the stainless steel electrodes of the unit which are used to detect her ECG and from this the device measures and displays her heart rate. The values of the two heart rates can then be compared by the midwife and used to discern whether or not the ultrasonic transducer is actually measuring the infant's heart rate reliably or the mother's heart rate in error. To this end it was decided to implement a mechanism in the Moyo unit which would verify that the mother's ECG was being measured reliably by the stainless steel un-gelled electrodes. This is done by measuring the contact impedance of the skin-electrode interface at both electrodes of the Mojo unit and detecting when the mother has pressed her fingers onto the electrodes. The circuit reported in this paper measures the contact impedance of each electrode independently and indicates when the state of contact of either electrode is unsatisfactory for the purposes of reliable ECG measurement, generating a visual alarm under this condition.

Fig. 1. The Handheld Moyo Unit

This work was supported in part by the Norwegian Research Council Grant No. ES506110 under the Safer Births Program.

M. J. Burke is with the Department of Electronic & Electrical Engineering, Trinity College, Dublin 2, Rep. of Ireland. (corresponding author, phone: +353-1-8961740; fax: +353-1-6772442; e-mail: mburke@tcd.ie).

C. Molloy is with the Department of Electronic & Electrical Engineering, Trinity College, Dublin 2, Rep. of Ireland. (e-mail: comolloy@tcd.ie).

H. Fossan is with Laerdal Medical AS. P.O Box 337, Tanke Svilandsgate 30, N-4002 Stavanger, Norway. (e-mail: helge.fossan@laerdal.no).

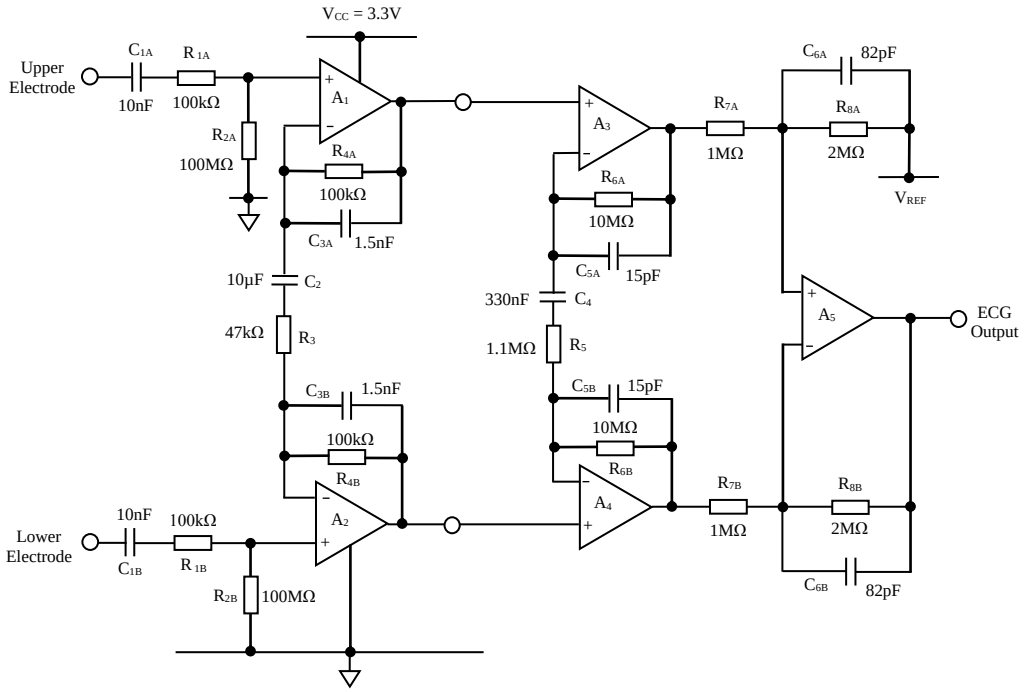

Fig. 2 Schematic Diagram of Existing ECG Amplifier

II. Background

A. Existing ECG Amplifier

The schematic diagram of the front-end ECG amplifier currently in use in the Moyo unit is shown in Fig. 2. This is a three-stage instrumentation ECG amplifier adapted from an earlier design by Burke & Gleeson [4,5] and later improved by Assambo & Burke [6-9]. The 46 dB of differential gain is split primarily between the first stage with 14.4 dB and the second stage with 25.6 dB while the third stage provides 6dB of the gain with differential-to-single-ended conversion. The input stage provides a high differential-mode and common-mode impedance of 100MΩ in order to preserve adequate common-mode-rejection-ratio (CMRR) when interfacing with high-impedance dry electrodes. The amplifier operates from a single 3.3V supply rail and the input stages are biased to a mid-rail voltage of 1.65V using a separate dc-to-dc convertor chip not shown in the schematic. The ESD protection elements are also omitted for clarity.

B. Electrodes

The electrodes used in the Moyo unit shown in Fig. 1 are made of stainless steel with either a polished or a matt surface, as these can easily be disinfected before use with an alcohol wipe. Electrical contact is made with the electrodes by the mother gripping the unit in both hands with her fingers placed on the electrode surfaces as shown. Only the firmness of the mother's grip determines the contact pressure. In order to obtain an indication of the contact impedance of these electrodes a method formerly reported by Baba & Burke [10, 11] was used to characterize the electrodes. The current source shown in Fig. 3 was used to inject a minute current of 2μA through the electrodes while being held by the user. The current was activated and then deactivated via the relay for stable periods of 20 – 50s. A 10 kHz sinewave signal was also used to allow the high frequency purely resistive components to be evaluated. A program in MATLAB (MathWorks Inc.) was then used to fit a two time constant C-R model shown in Fig. 4 to the recorded voltage waveforms and to determine the values of the individual components of the model.

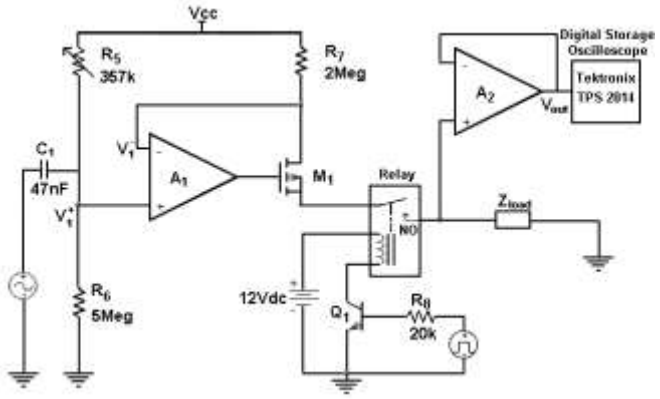

Fig. 3 Electrode Impedance Measurement Circuit

This was done for measurements made on a small number of subjects to get an initial idea of the scale and variation of electrode impedance to be expected. Only the passive components of the model were of interest in this instance and the dc polarization potentials were not measured. The ranges of values measured for each component of the model are listed in Table.1 below. Plots of the magnitude and phase as functions of frequency of a stainless steel electrode having a polished surface are shown in Fig. 5. Plots are shown for light and firm grips of the mother's fingers and for rise and fall phases of the injected current.

Table 1. Range of Values for the Electrode Model Elements

Element	Minimum	Maximum	Unit
$R_1 + R_3$	2.0	5.0	kΩ
R_2	23.2	267	kΩ
C_2	1.60	878	μF
R_4	36.0	380	kΩ
C_4	0.47	55.5	μF
τ_2	0.26	58.8	s
τ_4	0.13	8.62	s

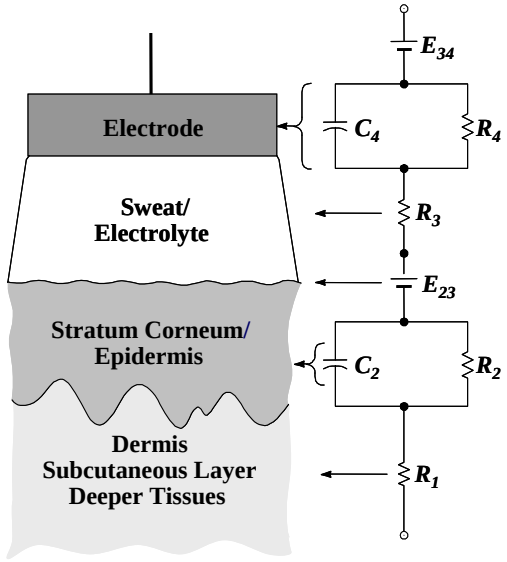

Fig. 4. An Equivalent Electrical Model of the ECG Electrode

It can be seen that the impedance varies considerably within the frequency range of the ECG signal. The magnitude falls off abruptly before 1 Hz and the phase falls off above 10 Hz. It can be seen that the magnitude of the impedance is less than 10 kΩ at frequencies above approximately 10 Hz. This is considerably lower than the input common-mode resistance of the amplifier or the protection resistor, R_1. This indicates that the signal levels involved in measuring the contact impedance of such electrodes are likely to be quite low.

III. System Design

A. Measurement Methodology

A block diagram of the electrode contact monitoring system and its placement in relation to the ECG amplifier is shown in Fig. 6. An oscillator and filter are used to provide a sinusoidal source signal at a frequency of 5 kHz with an amplitude of 1.5 V peak. Normally one would like the frequency of contact measurement to be much higher than the bandwidth of the ECG signal. However, the parasitic input capacitance of operational amplifiers causes a significant shunting effect at higher frequencies so the value of 5kHz was chosen to avoid this, while at the same time keeping the measurement frequency at least a decade above the ECG band. The sinewave is then buffered in both an inverting and a non-inverting amplifier to provide antiphase source signals. These signals are then fed through the common-mode input resistors of the ECG amplifier R_{2A} and R_{2B} to the electrode impedances

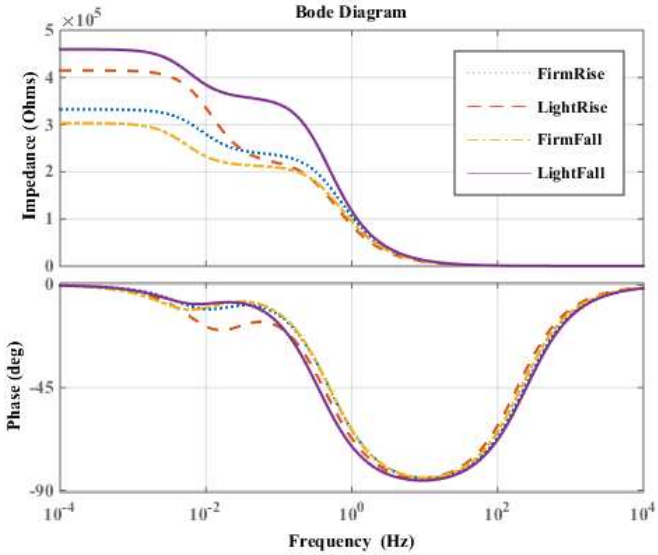

Fig. 5 Impedance of Polished Stainless Steel Electrode

Z_{EA} and Z_{EB}. This method of feeding the contact monitoring signal to the electrodes preserves the high common-mode impedance of the amplifier input and consequently the CMRR. The first stage of the ECG amplifier is also used to provide initial gain for the contact monitoring signal. Band-pass filters centred at 5 kHz are used to extract the contact monitoring signal at the differential outputs of the first stage of the ECG amplifier. The signals at the output of the upper and lower band-pass filters are then fed into half-wave rectifiers on each side so that an indication of the degree of contact of each electrode with the mother's body is obtained. With good contact the signal level detected from each electrode at the input of the ECG amplifier is of the order of 1–2 mV and when amplified and filtered is raised to approximately 500 mV in magnitude. This means that a definitive signal is available to the following pair of threshold detectors for decision making on the quality of electrode contact with the mother's body. Finally, the outputs of the threshold detectors are used to drive corresponding LEDs to indicate inadequate contact at either electrode.

B. Signal Generation and Injection

A schematic diagram of the circuit used to generate the source signal needed and to inject it through the electrodes is shown in Fig. 7. An astable multivibrator is formed around the op-amp A_6, which generates a square-wave signal at 5 kHz. A more triangular shaped waveform is obtained by taking the output oscillator signal from the top of the capacitor C_7, where an exponential charging/discharging voltage is present, rather than from the output of the op-amp itself. This is then filtered in the multiple-feedback band-pass filter built around op-amp A_8 to give an almost pure sinewave as the source signal for electrode contact measurement. This provides a sinewave with amplitude of 1.5V. The sinewave is then passed through two buffer amplifiers, a non-inverting unity-gain stage built around

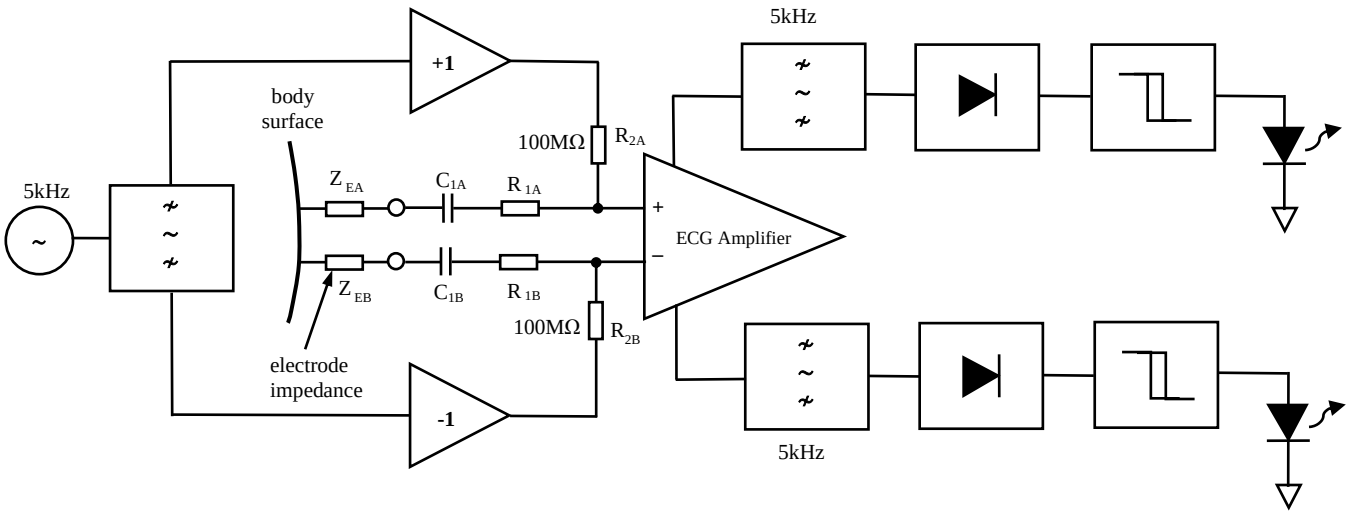

Fig. 6 Block Diagram of the Electrode Contact Monitoring System

op-amp A_9 and a unity-gain inverting stage built around op-amp A_{10}, which also have mid-rail bias voltages. The in-phase component is fed to the upper electrode point via the upper-channel common-mode input resistor R_{2A}. The inverted component is fed to the lower electrode contact point via the lower-channel common-mode resistor R_{2B}. The use of antiphase components allows the signal developed on the mother's body to be kept close to zero. The levels of 5 kHz signals developed at the input terminals of the ECG amplifier are those developed across the contact impedances of each electrode namely, Z_{EA} and Z_{EB}. With good contact and low skin-electrode impedance these signal levels will be extremely small as the resistor R_2 forms a potential divider with the electrode contact impedance, Z_E, at each terminal of the amplifier. In fact, most of the 5 kHz signal present is actually developed across the protection resistor R_1 in each case. This has a value of 100 kΩ, which is much greater than the contact impedance of the electrode itself. Under normal conditions with good electrode contact the signal at 5 kHz is of the order of 1 mV amplitude. If maximum electrode contact impedance

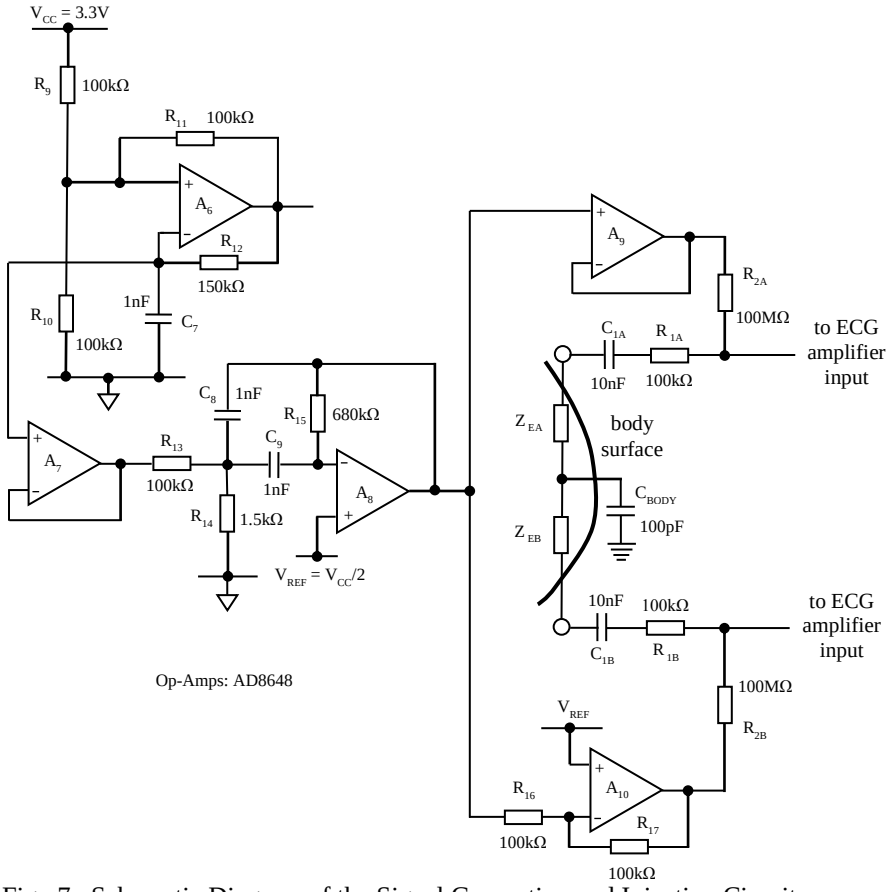

Fig. 7 Schematic Diagram of the Signal Generation and Injection Circuitry

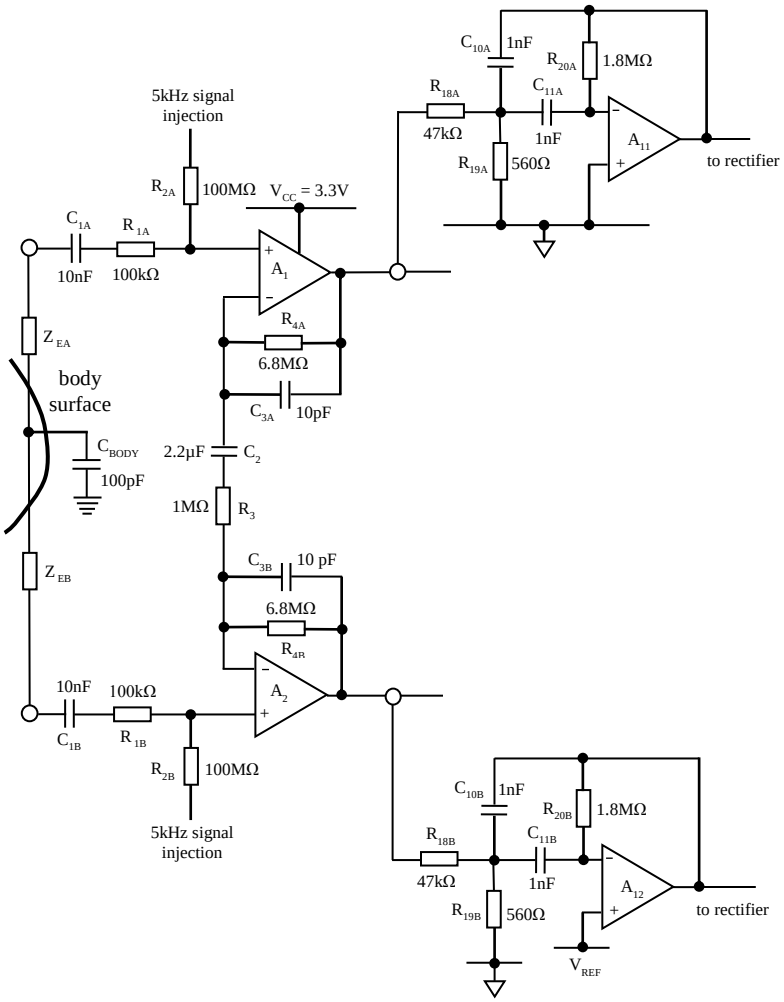

Fig. 8 Schematic Diagram of the Signal Extraction Circuitry

is set at 200 kΩ, which is twice the typical value of the resistor, R_1, then the maximum expected signal with good electrode contact appearing at the input of the ECG amplifier is then of the order of 3 mV.

C. Signal Extraction

It was decided to use the front-end stage of the ECG amplifier to provide the first phase of amplification for the contact monitoring signal. To this end the gains of the three stages of this amplifier were revised so that the first and second stage gains are now 23 dB and the third stage has unity gain. The revised component values set the 3 dB lower cut-off frequency at 0.67 Hz as required by the international standards for clinical heart-rate monitoring [12], while at the same time avoiding the use of electrolytic capacitors and increasing the CMRR by 6 dB. The upper cut-off frequency of the first stage was set to 10 kHz while those of the second and third stages are 250 Hz.

The electrode contact monitoring signals are extracted from the outputs of each side of the first stage of the ECG amplifier using band-pass filters built around op-amps A_{11} and A_{12}. These filters are multiple-feedback structures having a centre frequency of 5 kHz, a gain of 26 dB at this frequency and a Q-factor of 20. This provides an overall gain of 49 dB or a factor of 280 to the signal developed across the resistor R_1 and the electrode impedance Z_E in series. The output signal level from the filters with good contact is of then of the order of 150 mV. With poor electrode contact impedance of 200kΩ, this rises to approximately 450 mV peak.

D. Signal Rectification and Detection

A schematic diagram showing the rectification and threshold detector circuit is shown in Fig. 9. The output sinewave from the band-pass filter channel is fed into a precision half-wave rectifier in each channel built around op-amps A_{13} and A_{14}. The rectification process is inverting and includes envelope detection of the sinewave by means of the charge storage circuit composed of resistor R_{23} and capacitor C_{12}, having a time-constant of 0.1s. Further smoothing is provided by resistor R_{27} and capacitor C_{13} to reduce the residual ripple. This provides a steady-state voltage level representing the amplitude of the recovered sinewave at 5 kHz. The rectified level is negative-going with respect to the reference voltage of half the supply, V_{REF} = 1.65V. Therefore, at the limit of poor electrode contact, the output voltage of op-amp A_{13} or A_{14} falls to 1.2 V.

Finally, the rectified voltages in each channel are fed into threshold detectors built around op-amps A_{15} and A_{16}. The

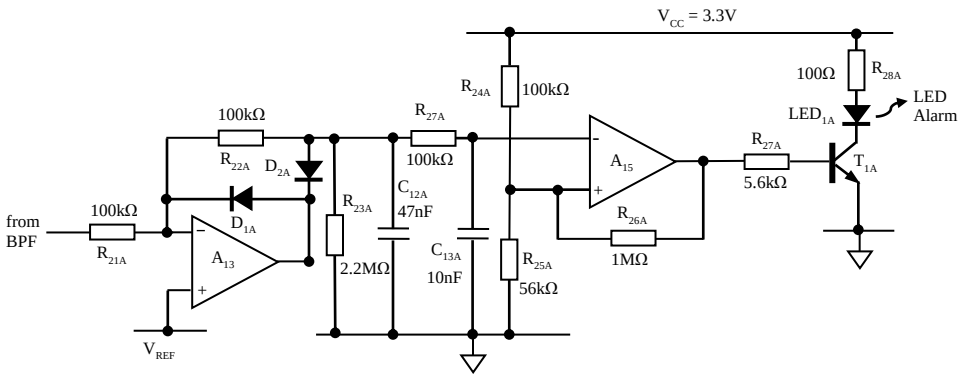

Fig. 9 Schematic Diagram of the Rectification and Threshold Detection Circuitry

reference voltage of each threshold detector is set at 1.18 V relative to ground by resistors R_{24} and R_{25} with approximately 50 mV of hysteresis added by the positive feedback provided by resistor R_{26}. The action of the threshold detectors is also inverting. Consequently, when the rectified 5 kHz signal level reaches a threshold of 470 mV below V_{REF} or 1.18 Vdc, the op-amp acting as a comparator changes state and its output goes from 0 V associated with good electrode contact, to the supply voltage of 3.3 V associated with poor electrode contact. This HI output voltage of the op-amp is then used to feed a bipolar transistor based light-emitting-diode (LED) driver that provides a current of 10 mA to the activated LED. This level of current provides sufficient contrast of the light level to allow clear determination of the ON/OFF state of the LED.

IV. System Verification

A schematic diagram showing the entire ECG amplifier and electrode contact monitoring circuit is given in Fig. 10. Operation of the electrode contact monitoring system was simulated using MultiSim (National Instruments Corp.) The entire schematic of Fig. 10 was entered into the schematic editor for simulation.

Table 2 Values of Signal Levels vs Electrode Resistance

$\|Z_E\|$	V_{A11} (Vpk)	V_{A12} (Vpk)	V_{R23A} (Vdc)	V_{R23B} (Vdc)	V_{A15} (logic)	V_{A16} (logic)
1 kΩ	0.17	0.17	1.49	1.49	LO	LO
2 kΩ	0.17	0.17	1.49	1.49	LO	LO
5 kΩ	0.17	0.17	1.49	1.49	LO	LO
10 kΩ	0.18	0.18	1.48	1.48	LO	LO
20 kΩ	0.19	0.19	1.46	1.46	LO	LO
50 kΩ	0.24	0.24	1.41	1.41	LO	LO
100 kΩ	0.33	0.33	1.34	1.34	LO	LO
200 kΩ	0.48	0.48	1.17	1.17	HI	HI
500 kΩ	0.96	0.96	0.722	0.722	HI	HI
1 MΩ	1.63	1.63	0.519	0.519	HI	HI
2 MΩ	1.65	1.65	0.503	0.503	HI	HI
5 MΩ	1.65	1.65	0.503	0.503	HI	HI
10 MΩ	1.65	1.65	0.501	0.501	HI	HI

A. Contact Monitoring Performance

In the first instance the electrodes were modelled as pure resistors. The value of the resistors were varied in non-uniform steps from 1 kΩ to 10 MΩ and the signal level at the output of the filters, V_{A11}, V_{A12}, the half-wave rectifiers, V_{R23A}, V_{R23B} and the threshold detectors, V_{A15}, V_{A16}, were monitored in both upper and lower channels. These levels are shown in Table 2 and can be seen to be a little lower than the design values due to the loading effect of op-amp input capacitance. It can also be seen that the threshold detector logic outputs, change state at a value of electrode resistance between 100 kΩ and 200 kΩ which is considered acceptable.

As a more practical test, a set of electrode models identical to that of Fig. 4 were created with the component values measured during the tests outlined in Section II B. This gave 24 electrode models with different component values as given in Table 3. All of the electrode models have good electrode contact as indicated by the output logic states of the threshold detectors. The resistors R_{EA} and R_{EB} are the values of additional resistance which needed to be added in series with the electrodes to cause the respective threshold detectors to change state and activate the LEDs. All of these values are in the region of 100 kΩ – 120 kΩ. These resistance values were established independently for the two channels indicating that they are closely matched. Definitive measurement of electrode contact impedance of the rectification and threshold detection stages can be appreciated from the waveforms shown in Fig. 11, where the threshold voltage is used as representative of the logic output of the comparator op-amp A_{15}. The waveforms shown correspond to an electrode impedance of 200 kΩ. It can be seen that the decision on the poor state of electrode contact is reached within 5 ms in this case.

Mote Carlo simulations were carried out to establish the extent of the variations in important circuit properties such as the resonant frequency and Q-factor of the band-pass filters, for example, under the influence of manufacturing tolerances of the components. Table 4 shows the extremes of variation of a selection of properties of the circuits within the electrode impedance measuring path as well as the ECG amplifier for 500 Monte Carlo iterations. The cumulative effect of these variations affecting any single operation was within ±5%, which was considered acceptable.

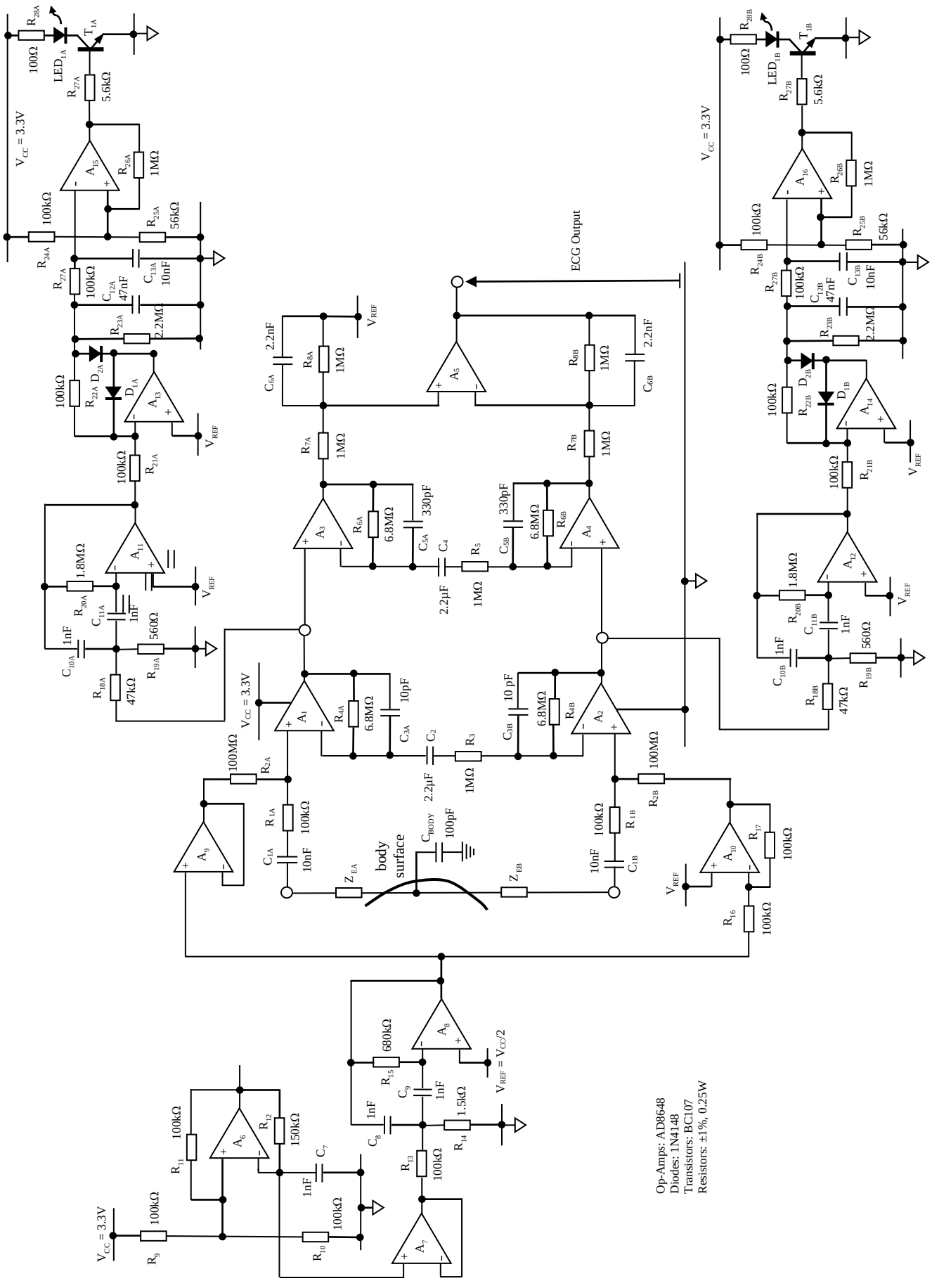

Fig. 10 Schematic Diagram of Combined ECG Amplifier and Electrode Contact Monitor

Table 3 Values of Signal Levels Recorded for a Range of Electrode Models

No	R_1+R_3 (kΩ)	R_2 (kΩ)	C_2 (μF)	τ_2 (s)	R_4 (kΩ)	C_4 (μF)	τ_4 (s)	V_{A11} (mVpk)	V_{A12} (mVpk)	V_{R23A} (Vdc)	V_{R23B} (Vdc)	V_{A15} (logic)	V_{A16} (logic)	R_{EA} (kΩ)	R_{EB} (kΩ)
1	5	97.0	203	19.7	235	1.98	0.47	0.17	0.17	1.5	1.5	LO	LO	110	110
2	5	94.3	383	36.1	213	1.56	0.33	0.16	0.16	1.5	1.5	LO	LO	110	110
3	4	81.6	164	13.4	83.4	10.9	0.91	0.16	0.16	1.5	1.5	LO	LO	120	120
4	4	95.4	464	42.6	81.3	18.8	1.53	0.16	0.16	1.5	1.5	LO	LO	120	120
5	2	94.3	172	16.2	41.8	11.3	0.47	0.11	0.11	1.55	1.55	LO	LO	110	110
6	2	101	277	28.1	46.5	7.0	0.33	0.11	0.11	1.55	1.55	LO	LO	110	110
7	5	198	84.7	0.17	219	1.85	0.41	0.16	0.16	1.5	1.5	LO	LO	120	120
8	5	104	270	28.1	355	1.49	0.53	0.16	0.16	1.5	1.5	LO	LO	120	120
9	4	93.6	254	23.8	63.7	17.7	1.13	0.16	0.16	1.5	1.5	LO	LO	120	120
10	4	106	470	49.8	63.7	21.9	1.40	0.16	0.16	1.5	1.5	LO	LO	120	120
11	2	111	10.5	11.7	43.3	7.51	0.33	0.11	0.11	1.55	1.55	LO	LO	110	110
12	2	111	217	24.1	46.8	7.50	0.35	0.11	0.11	1.55	1.55	LO	LO	110	110
13	5	59.3	116	6.9	132	20.3	2.67	0.16	0.16	1.5	1.5	LO	LO	120	120
14	5	55.7	336	18.7	162	2.36	0.38	0.16	0.16	1.5	1.5	LO	LO	120	120
15	4	79.1	381	30.1	142	6.27	0.89	0.16	0.16	1.5	1.5	LO	LO	110	110
16	4	45.3	576	26.1	124	4.96	0.62	0.16	0.16	1.5	1.5	LO	LO	110	110
17	2	44.5	541	24.1	43.2	6.39	0.28	0.11	0.11	1.55	1.55	LO	LO	120	120
18	2	32.1	784	25.2	61.4	6.29	0.39	0.11	0.11	1.55	1.55	LO	LO	120	120
19	5	144	116	16.7	247	1.49	0.37	0.16	0.16	1.5	1.5	LO	LO	120	120
20	5	67.8	201	13.6	227	2.21	0.50	0.16	0.16	1.5	1.5	LO	LO	110	110
21	4	41.6	504	21.0	64.8	8.2	0.53	0.16	0.16	1.5	1.5	LO	LO	110	110
22	4	42.3	590	24.9	66.8	11.0	0.74	0.16	0.16	1.5	1.5	LO	LO	120	120
23	2	43.8	753	33.0	50.7	14.5	0.74	0.11	0.11	1.55	1.55	LO	LO	110	110
24	2	33.6	633	21.3	49.5	10.5	0.52	0.11	0.11	1.55	1.55	LO	LO	110	110

Table 4 Variation in Circuit Parameters with Component Manufacturing Tolerance

% tolerance	Ocillator		Band-Pass Filter 1				ECG Amplifier	Band-Pass Filter 2				Threshold Detector
	f_0	A_0	f_0	H_0	Q	BW	G	f_0	H_0	Q	BW	V_{TH}
R ±1% C ±5%	±4.8%	±0.4%	±4.0%	±3.7%	±0.6%	±3.0%	±1.6%	±3.8%	±3.8%	±0.8%	±3.1%	±0.9%
R ±1% C ±1%	±1.8%	±0.4%	±1.0%	±1.5%	±0.8%	±1.2%	±1.1%	±1.1%	±1.5%	±0.7%	±1.0%	±0.8%

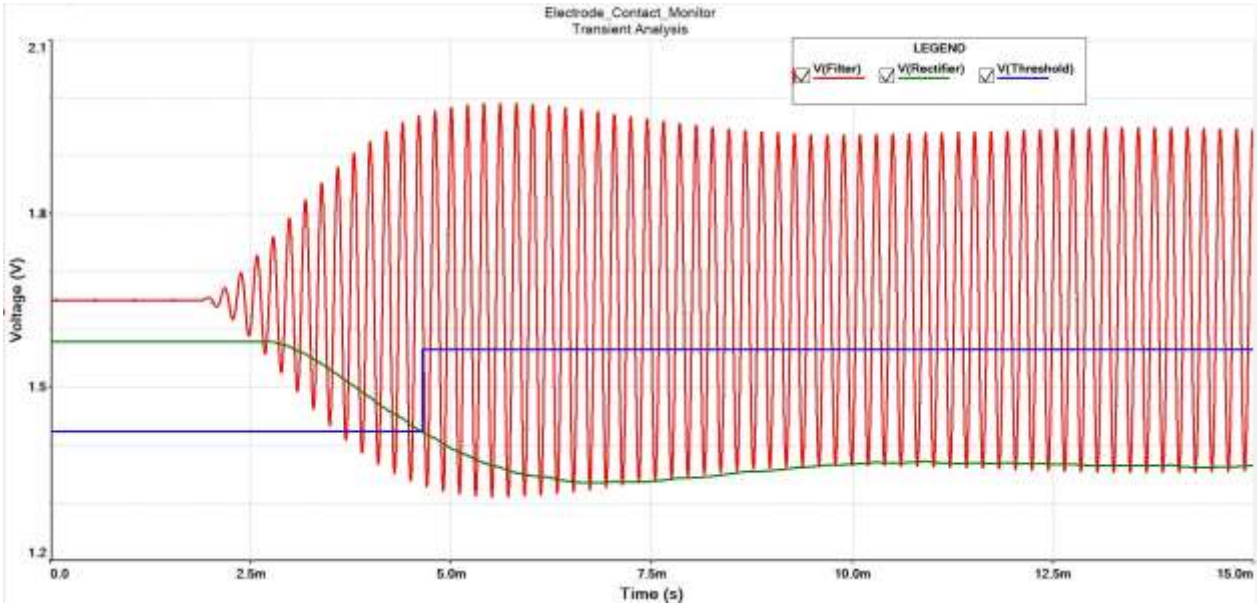

Fig. 11 Waveforms Showing Operation of the Band-Pass Filter, Rectifier and Threshold Detector Circuitry

B. *ECG Amplifier Performance*

Following the modifications made to the ECG amplifier its performance was also verified to ensure that no detrimental changes had occurred and that it still met the requirements. Plots of the gain and phase vs. frequency responses of the ECG amplifier are shown in Fig. 12. The mid-band gain can be seen to be 52 dB in the plot, but this is because the output voltage was taken relative to only one of the differential input source and consequently appears 6 dB higher than the correct value of 46 dB. The lower cut-off frequency can be seen to be 0.67 Hz as required. The plots also include the response of a subsequent 4th-order low-pass filter having a cut-off frequency of 40 Hz, which is evident from the plot.

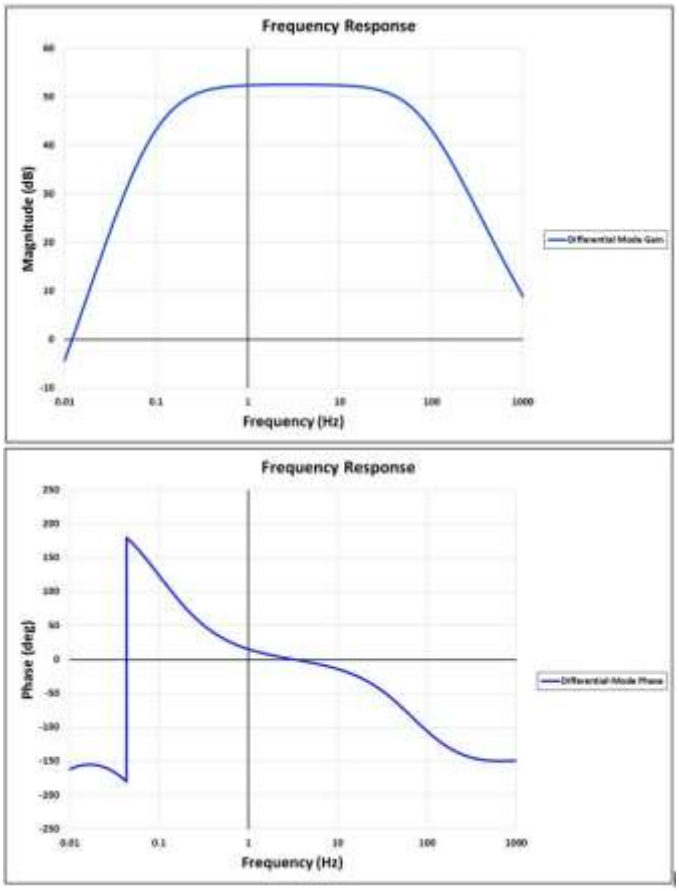

Fig. 12 ECG Amplifier Gain and Phase vs Frequency

The common-mode rejection ratio of the simulated circuit was also obtained and is shown in Fig. 13. The plot shows a mid-band CMRR of over 90 dB. This is because the particular plot shown was obtained without mismatch in the passive components in the circuit and only accounts for the finite CMRR of the op-amps.

Waveforms showing the output voltage at each stage of the ECG amplifier and the subsequent filter are shown in Fig. 14 for steady-state conditions. The low-level signal on the lower trace is the output signal of the first stage of the amplifier, measured differentially to allow it to be observed. This shows a low-level ECG signal combined with a low-level 5 kHz signal, as the electrode contact is of good quality. The second

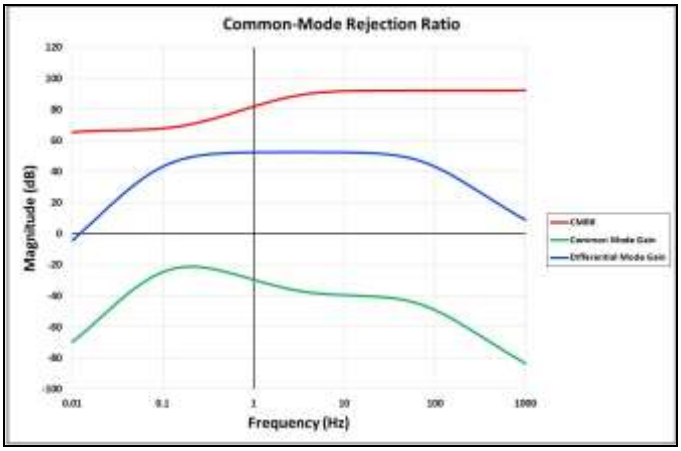

Fig. 13 Amplifier Common-Mode Rejection vs Frequency

signal on the lower trace is the output signal from the second stage of the amplifier, again measured differentially for observation. It can be seen that the ECG signal has been amplified considerably in this stage, while the 5 kHz signal has been slightly attenuated. The signal on the upper trace, appearing earlier in time, is the output of the 3rd differential-to-single ended conversion stage of the amplifier, having unity gain. This can be seen to be the ECG signal with the 5 kHz signal virtually removed. The final signal on the upper trace, appearing later in time, is the output of the 4th order filter. Despite the low value of 40 Hz as the cut-off frequency the ECG signal appears virtually undistorted with a slight delay which does not introduce any error into the measured heart rate in the Moyo unit.

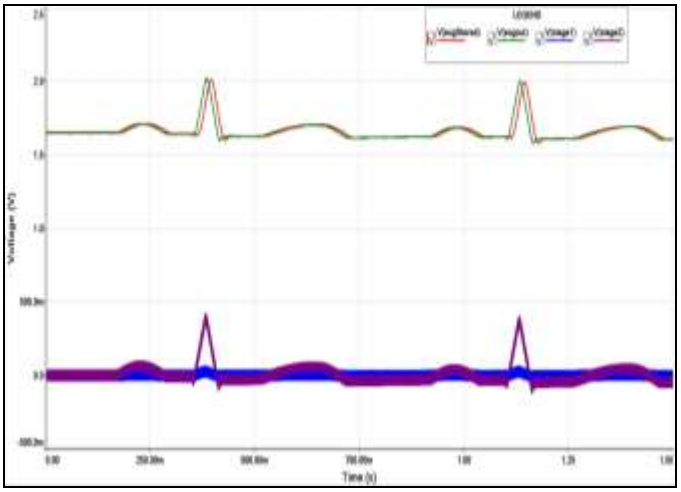

Fig. 14 Waveforms of the Output Voltages of the Amplifier

The final waveforms shown in Fig. 15 are those of the output voltages of the final stage of the ECG amplifier and that of the low-pass filter, representing the transient conditions which prevail immediately after power-up. It can be seen that the bias levels become stable within 3 seconds and that the ECG signal is available almost immediately. The detection algorithm in the Moyo unit is able to obtain a heart rate within 2 seconds of power-up.

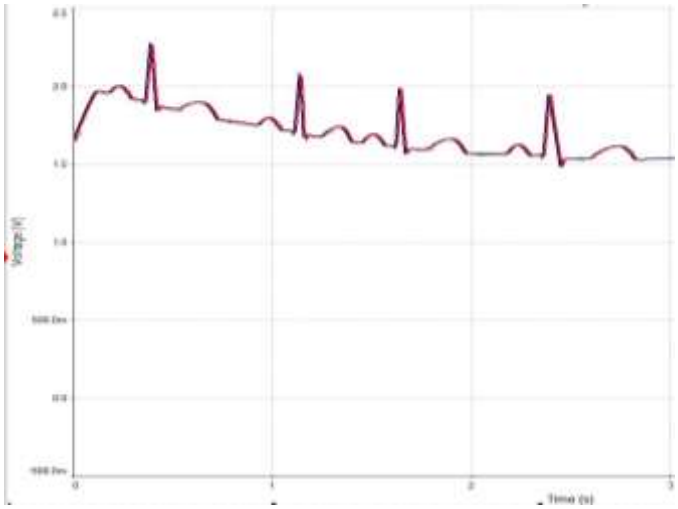

Fig. 15 Waveforms of the Output Voltages on Power-Up

V. Conclusion

The results presented above verify the functionality of the circuit design from the simulation point of view. A hardware prototype has recently been recently been constructed photos of both sides of the circuit board are shown in Fig. 16. The prototype is currently undergoing bench testing. Initial observations give the impression that some fine tuning of the threshold detector circuit is required to bring the design to perfection.

References

[1] http://www.saferbirths.com

[2] http://www.who.int/en

[3] Murray, M. M. "Maternal or Fetal Heart Rate? Avoiding Intrapartum Misidentification" J. Obstet. Gynecol. & Neonatal Nurs., vol 33, pp33-104, 2004.

[4] M. J. Burke, D. T. Gleeson "An Ultra-Low-Power Preamplifier for Pasteless Electrocardiograpy" *Proc. 6th IEEE Int. Conf. Electronics, Circuits & Systems*, Cyprus, pp 616 – 619, 1999.

[5] M. J. Burke, D. T. Gleeson "A Micropower Dry-electrode ECG Pre-amplifier" *IEEE Trans. Biomed. Eng.*, vol. 47, pp155-162, 2000.

[6] M. J. Burke, C. Assambo "An Improved Micro-power Pre-amplifier for Dry-electrode ECG Recording", *Proc. 11th WSEAS Int. Conf. Circuits, Systems, Communications & Computers*, Crete, Paper No. 561-286, July 2007.

[7] Assambo, C., Burke, M. J. "An Improved Very-Low Power Preamplifier for Use with Ungelled Electrodes in ECG Recording*" NAUN Int. J. Biol. & Biomed. Eng.*, vol. 1, pp. 25-35, 2007.

[8] Burke, M. J., Assambo, C. "An Ultra-Low Power Dry-Electrode ECG Amplifier Having Optimized Low-Frequency Response and CMRR" *Proc. 16th WSEAS Int. Conf. Circuits, Systems, Communications & Computers*, Kos, Paper No. 68101-025, July 2012.

[9] Assambo, C., Burke, M. J. "An optimized High-Impedance Amplifier for Dry-Electrode ECG Recording" *NAUN Int J. Circuits, Systems & Signal Processing*, vol. 6, pp. 332–341, 2012.

[10] Baba, A., Burke, M. J. "Electrical Characterization of Dry Electrodes for ECG Recording" *Proc. 12th WSEAS Int. Conf. Circuits, Systems, Communications & Computers*, Crete, Paper No. 591-226, July 2008.

[11] Baba, A., Burke, M. J. "Measurement of the Electrical Properties of Ungelled ECG Electrodes" *NAUN Int. J. Biol. & Biomed. Eng.*, vol. 2, pp. 89-97, 2008.

[12] EU Commission, Medical electrical equipment Part 2-27: Particular requirements for the safety, including essential performance, of electrocardiographic monitoring equipment, *IEC Std. IEC60 601-2-27*: 2011, 3rd ed., March 2011.

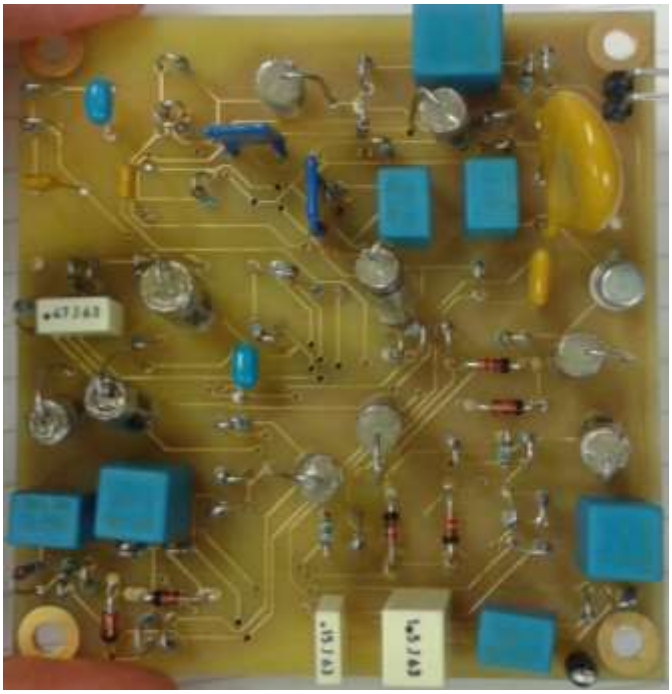

Fig. 16 Photos of Both Sides of the Circuit Board